Charge-density waves studied with the use of a scanning tunneling microscope

C. G. Slough, W. W. McNairy, and R. V. Coleman
Department of Physics, University of Virginia, Charlottesville, Virginia 22901

B. Drake and P. K. Hansma
Department of Physics, University of California Santa Barbara, Santa Barbara, California 93106
(Received 13 January 1986)

Scanning tunneling microscope (STM) images of charge-density waves (CDW's) formed in the layered-structure dichalcogenide crystals TaS_2 and $TaSe_2$ have been obtained with a microscope operating in a bath of liquid nitrogen. In $1T$-TaS_2 and $1T$-$TaSe_2$ the images show a hexagonal network of mounds spaced at the CDW wavelength, $\lambda_{CDW}=\sqrt{13}a_0$ where a_0 is the atom spacing. The microscope tip deflection in the constant-current mode is extremely large (~ 2 Å) which gives an image of the $1T$-phase surface which is completely dominated by the CDW. In $2H$-$TaSe_2$ the CDW is much weaker and careful adjustment of the microscope parameters can give STM images which show superimposed modulations at the atomic wavelength and at the CDW wavelength, $\lambda_{CDW}=3a_0$. However, in general the STM scans of the $2H$ phases are dominated by patterns at the atomic wavelength. At 77 K the $4Hb$-TaS_2 crystals produce STM images with some areas showing atoms only and others showing CDW's only consistent with the existence of a CDW in the octahedral layers only. The STM results for all of the phases of TaS_2 and $TaSe_2$ are consistent with the expected variations in the CDW formation and electron transfer as determined by calculation and experiment. However, the unusually large deflection of the tunneling tip caused by the stronger CDW amplitudes in the $1T$ phases needs further analysis.

I. INTRODUCTION

Scanning tunneling microscopy (STM) is developing into a powerful tool for the study of surface topography on an atomic scale.[1] Since it responds to a charge-density variation as well as to the surface topography it also has great potential for the study of electronic structure near the surface. Spectroscopic information on the surface density of states as well as on the modification produced by impurities or imperfections can also be obtained in principle.

The formation of charge-density waves (CDW's) in metallic conductors represents a strong modification of the band structure and electronic density of a metal without a major change of the crystal structure. A periodic lattice distortion accompanies the formation of a CDW, but this generally corresponds to changes in the atom positions of less than a few tenths of an angstrom[2] and only a slight distortion of the original high-temperature crystal structure occurs.

In this paper we present studies of the CDW's observed in the layered-structure transition-metal dichalcogenides[2,3] using a scanning tunneling microscope operating at 77 K in a bath of liquid nitrogen. The studies reported here are to the various phases of TaS_2 and $TaSe_2$, but can be easily extended to the whole class of such compounds. These are particularly well suited to tunneling microscopy since they grow as close-packed three-atom-layer sandwiches of metal and chalcogenide atoms stacked with a van der Waals gap between each three-layer unit. They therefore cleave quite easily leaving a nearly atomically flat highly perfect surface for study. Preliminary results on the CDW in $1T$-TaS_2 were reported by Coleman *et al.*[3]

The results show that the charge-density rearrangement due to the CDW formation is easily detectable with the STM and represent one more powerful application of the STM to surface problems. Milestones in this development have included profiling of grating surfaces,[4,5] observation of steps one atom high,[6–8] detailing of the atomic positions in semiconductor reconstructions,[9,10] demonstration of small-scale variation in the superconducting energy gap at the surface of a thin film,[11] observation of single atoms in a close-packed layer,[12] and spectroscopic imaging.[13]

In the sections below we summarize the experimental techniques, present the scanning images of both atoms and CDW's, discuss the results in terms of the large amount of information already developed from other experiments and calculations relating to the CDW phases in these materials, and make some comments on future developments. Details on the construction of the microscope have been published in Ref. 14, so that we give here an abbreviated version of the microscope construction and operation.[14]

II. EXPERIMENTAL TECHNIQUES

A. Construction and operation of the STM

The tunneling microscope used in these experiments is a hybrid design utilizing features of the IBM Zurich design[6–9] and squeezable tunnel junctions.[15–18] The x-y translator design is shown in Fig. 1 and is cut from a block of Channel 5400 piezoelectric material.[19] Spacers

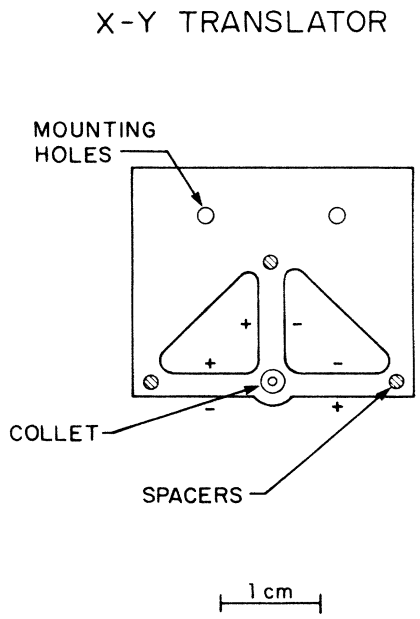

FIG. 1. x-y translator used to move the collet which holds the tunneling tip. The + and − signs indicate the direction of poling on the two sections of the x arm and on the single y arm. The x-y translator is cut from a single piece of Channel 5400 piezoelectric material 4 mm thick.

1.5 mm in diameter and 1.2 mm in height are mounted on the translator and locate the z translator above the x-y translator. The collet, made from a 2-56 brass screw, holds the scanning tip which is made from a $Pt_{0.8}Ir_{0.2}$ wire 0.5 mm in diameter. The signs along the arms of the translator in Fig. 1 signify the poling directions.

The x motion is generated by applying a voltage so that the electric field is in the direction of poling for one arm and opposite to the direction of poling for the arm across from it. Thus, one arm expands and one contracts, moving the collet and tip to one side relative to the spacers, while maintaining the total distance between the spacers the same. The motion is of order 4.3 Å/V at room temperature and 3.3 Å/V at liquid-nitrogen temperature.

The y motion is generated by applying voltage to the one remaining y translation arm which moves the collet and tip by bending the x translation arms. The calibration for the y axis is roughly the same as for the x axis.

The most direct way to calibrate the translator is in terms of an atomic image of a known structure. The piezoelectric arm may also be calibrated by attaching a mirror and including it in a Michelson interferometer, or by attaching a capacitor plate and including it in a capacitance bridge (e.g., a type 1615 General Radio capacitance bridge). These methods are in reasonable agreement with data supplied by the manufacturer.

The z translator is a half circular disk made of Channel 5800 piezoelectric material. It is 3 cm in diameter and composed of two layers each 1 mm thick glued together with epoxy. We have also experimented with layers 0.5 mm thick and, more recently, 1.5 mm thick. The thicker the layers the greater the rigidity, but the smaller the range since the motion is proportional to one over the square of the thickness. For 1 mm thick layers the motion is roughly 60 Å/V at room temperature and 36 Å/V at liquid-nitrogen temperature based on the manufacturer's values for d_{31}, g_{31}, and ε_{33} followed by extrapolation to 77 K using another manufacturer's data[20] for similar materials.[21]

Figure 2 shows a side and sectional view of the translator assembly. The z translator is shown in the operating position with the sample mounted on the bottom surface. Typically the sample is mounted with fast drying glue (Duco) or varnish (GE7031) on a glass cover slip which is glued to the bimorph. Section A-A shows the collet with the scanning tip, drill blank spacer and 0.5 UNM (unified minature) threaded wire. The collet is made with a press fit on the 0.5 mm diameter $Pt_{0.8}Ir_{0.2}$ tip. The press fit allows for smooth advancement of the tip position as the threaded wire and drill blank are advanced. When the threaded wire and drill blank are retracted the tip will retain its position. The drill blank is used to isolate the tip from the rotation of the threaded wire. Details of the entire support assembly and adjustment procedures can be found in Ref. 14.

The liquid-nitrogen bath is provided using a double Dewar system with liquid nitrogen in both the inner and outer Dewars. The system uses two independent vibration-isolation systems. The support frame and Dewar system are suspended from the ceiling with latex tubing stretched enough that the resonant frequency is less than 0.5 Hz. The second vibration isolation is provided by a long steel spring which extends and finally supports the microscope in the liquid-nitrogen bath.

A mechanical pump is used to evacuate a bell-jar assembly at the top of the Dewar system before the microscope is slowly lowered into the liquid-nitrogen bath and allowed to cool. After the whole assembly has reached

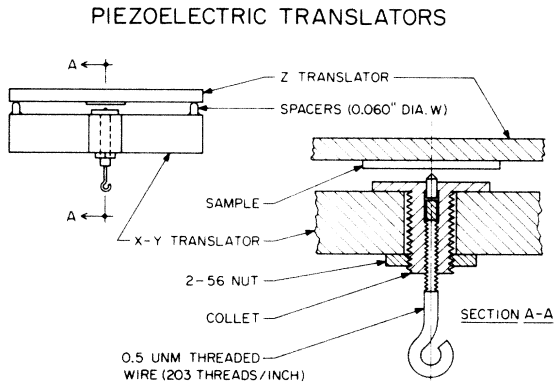

FIG. 2. Side view of the z translator supported above the x-y translator by the indicated spacers. The z translator is a bimorph which warps up and down with the applied voltage in order to keep the tip to sample distance constant. The section on the right shows detail of the collet and screw used for the tip adjustment. The z translator is a half circular disk of Channel 5800 material 3 cm in diameter and composed of two layers each 1 mm thick.

steady state the liquid nitrogen in the inner Dewar does not boil visibly and has not been demonstrated to contribute noise to the tunneling image. Further design development may decrease turbulence and improve image quality. Further description and diagrams of the main assembly can be found in Ref. 14.

The microscope scans are made at constant tunneling current maintained by a logarithmic integrating error amplifier. The tip-to-sample current is monitored by measuring the voltage across a 1 MΩ series resistor with a Princeton Applied Research 113 preamplifier operated at a gain of 100. The high-voltage amplifiers driving the piezoelectric translators were home built, but alternate commercial amplifiers could also be used. The tunneling current is maintained in the range 1—10 nA and the bias between the tunneling tip and sample is set in the range 7—35 mV in standard operation.

The scanning sweep in the x direction was usually made at a rate of 10 Hz. The y motion was adjusted to give a reasonably high density, but still resolvable number, of sweeps across the entire storage oscilloscope screen. The z motion is superimposed on the y motion so that a pseudo-three-dimensional image results. A complete scan is made in 5—30 sec., and the screen is then photographed with a Polaroid camera. One clear improvement for the microscope will be a computerized data-collection and image-processing system.

B. Crystal growth and surface preparation

The crystals used for this investigation were grown by the method of iodine-vapor transport from stochiometric prereacted powders sintered at 900 °C. The powders were then placed in quartz growth tubes with iodine vapor condensed into the tube before sealing. The $1T$-phase crystals were grown at temperatures above 900 °C in a temperature gradient of ~50 °C for several weeks and then quenched to room temperature where the $1T$ phase remains stable indefinitely. Both $1T$-$TaSe_2$ and $1T$-TaS_2 grow as flat shiny gold-colored platelets on the order of $2\times2\times0.2$ mm^3. The $2H$ and $4Hb$ phases can be grown at intermediate temperatures and only the $2H$ phase can be produced by slow cooling from the growth temperature. The $4Hb$-TaS_2 crystals were grown in a gradient of 720—700 °C for 4—5 weeks and then quenched to room temperature. The temperature gradients were applied over a length of ~10 cm.

Highly perfect crystals of $2H$-TaS_2 were grown by first growing the $4Hb$ phase and then slowly cooling the crystals over a period of 3 days to allow transformation to the $2H$ phase. For both the $4Hb$ and $2H$ phases the crystals were smooth grey-black or black metallic polyhedra of relatively high geometrical perfection.

The $2H$-$TaSe_2$ crystals were grown in a gradient of 770—750 °C for 2 weeks and cooled to room temperature over a period of 12 h. These crystals grew as thin platelets with mirror surfaces with the largest crystals of dimensions 1 cm × 1 cm × 0.5 mm.

The growth procedures were carried out with great care and highly perfect crystals resulted. This was confirmed by optical examination as well as by measurements of residual resistance ratios on the $2H$ and $4Hb$ crystals from the same batches as used for the tunneling microscopy. The residual resistance ratio, $\rho_{300\,K}/\rho_{4.2\,K}$, for these crystals were in the range 60—300. The purity and perfection of the metallic CDW phases grown by these methods have also been confirmed in measurements of large magneto-quantum oscillations[22,23] associated with the CDW Fermi surfaces.

After the crystal had been mounted on the z-axis piezoelectric translator it was cleaved by the Scotch-tape method just before mounting the translator in the microscope. Once the crystal has been mounted on the bimorph it can be cleaved a number of times for repeated STM studies on the same crystal. Most cleaves provide relatively large areas of atomically flat surface for scanning. Some cleavage steps are observed and an example of a step three atom layers high is shown in Fig. 3.

III. EXPERIMENTAL RESULTS

A. Imaging of CDW structure in the $1T$ phases

The charge-density-wave transitions in the $1T$ phases of $TaSe_2$ and TaS_2 produce substantial decreases in the conductivity and correspond to a major reduction in Fermi-surface area. Figures 4 and 5 show the resistivity parallel to the layers versus temperature for both the $1T$ and $2H$ phases of $TaSe_2$ and TaS_2. Although $1T$-TaS_2 has a more complex hysteretic transition than observed in $1T$-$TaSe_2$, both exhibit a commensurate CDW at 77 K with a CDW wavelength $\lambda_{CDW}=\sqrt{13}a_0$ with $a_0=3.346$ Å for $1T$-TaS_2 and $a_0=3.477$ Å for $1T$-$TaSe_2$. The CDW's forming in the $1T$ phases should be associated with large electron transfer and would be characterized by strong effects on the band structure. In the case of $1T$-TaS_2 this has been verified in a number of experiments and calculations to be summarized in Sec. IV.

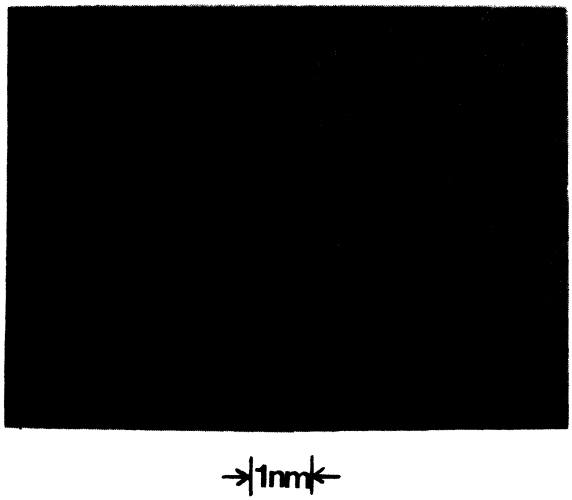

FIG. 3. STM image of a cleavage step on a $2H$-$TaSe_2$ crystal surface at 77 K. The step height is 17.0±2.1 Å corresponding to 3 atomic layers. The microscope was set for $I=2$ nA and bias voltage equal to 40 mV.

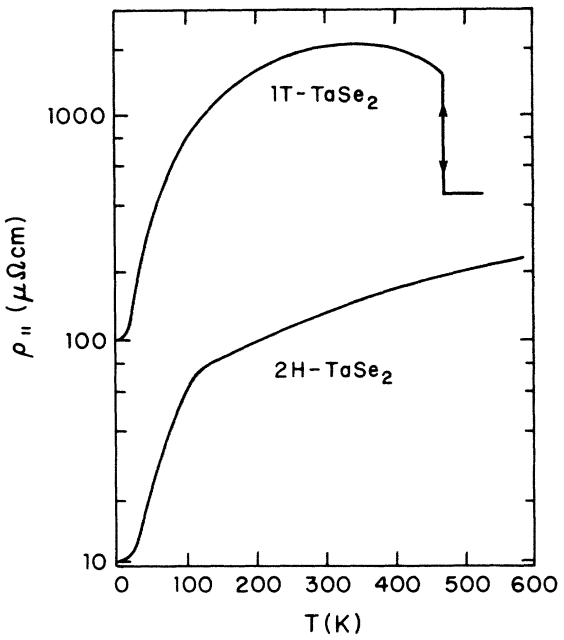

FIG. 4. Resistivity versus temperature for $1T$-$TaSe_2$ (upper curve) and $2H$-$TaSe_2$ (lower curve) measured parallel to the layers. $1T$-$TaSe_2$ shows an incommensurate-to-commensurate CDW transition at 473 K with a corresponding discontinuous resistance increase. $2H$-$TaSe_2$ shows the formation of a CDW with an onset temperature at 122.3 K. The resistance shows a change in slope below 120 K. Data are from Ref. 2.

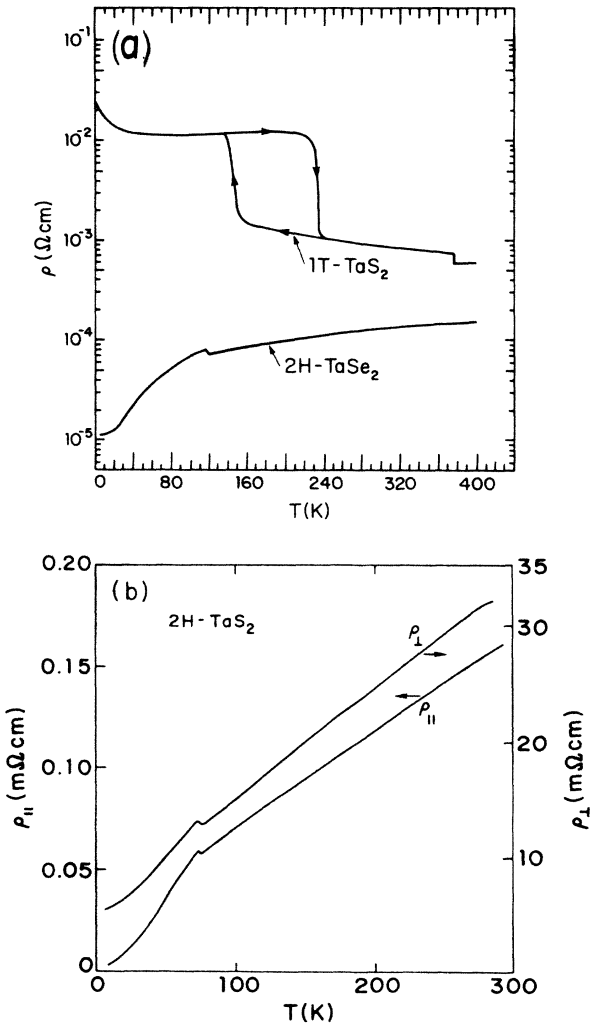

FIG. 5. (a) Resistance versus temperature for $1T$-TaS_2 (upper curve) and $2H$-$TaSe_2$ (lower curve) measured parallel to the layers. $1T$-TaS_2 shows a small discontinuity at 350 K where rotation of the CDW superlattice occurs. This is followed by a large hysteretic discontinuity centered at $\sim$200 K corresponding to a final rotation of the CDW into a commensurate phase. The $2H$-$TaSe_2$ resistivity curve was measured on a high-purity $2H$-$TaSe_2$ crystal and shows a small discontinuity at the CDW onset followed by a change in slope. Data are from Ref. 3. (b) Resistivity versus temperature for $2H$-TaS_2 measured both parallel and perpendicular to the layers. A small discontinuity occurs near 75 K corresponding to the onset of CDW formation. Data are from Ref. 23.

Scans with the tunneling microscope taken on $1T$-TaS_2 and $1T$-$TaSe_2$ are shown in Figs. 6 and 7. Freshly cleaved surfaces of both crystals show a pattern characteristic of a CDW modulation which completely dominates for all settings of the microscope. None of the 8—10 $1T$-phase crystals which have been run show the atomic spacing except possibly at locations near boundaries corresponding to some type of domain or phase inclusion. The periodic mounds correspond to a z-axis deflection of $\sim$2 Å and therefore represent an extremely strong perturbation of the tunneling characteristic by the CDW periodicity. The exact mechanism for this is not clear but possibilities will be discussed in Sec. IV. However, this observation is clearly consistent with the other evidence that the CDW is an extremely strong perturbation in the $1T$ phase.

In Figs. 6 and 7 the horizontal deflection is 6.6 Å per division on the graticule of the oscilloscope. The verticle deflection is 6.6 Å per division on the graticule of the oscilloscope plus $\approx$3.5 Å per division times the z motion. A majority of the scanning images presented in this paper have been recorded at the above magnification which allows good resolution of the structure and also gives a good view of the periodicity. Magnification, tunneling current, and bias voltage will be listed in the caption for each tunneling scan presented.

B. Images of CDW's and atoms in the $2H$ phases

In the case of $2H$-$TaSe_2$ and $2H$-TaS_2 the CDW transitions are at lower temperatures than observed in the $1T$ phases, and they exhibit only small resistance anomalies as shown in Figs. 4 and 5. Surface scans with the tunneling microscope show the atomic periodicity as the dominant pattern as shown for $2H$-$TaSe_2$ in Fig. 8. The z-axis deflection in this case corresponds to $\sim$0.2 Å which is in the range which might be expected from variations

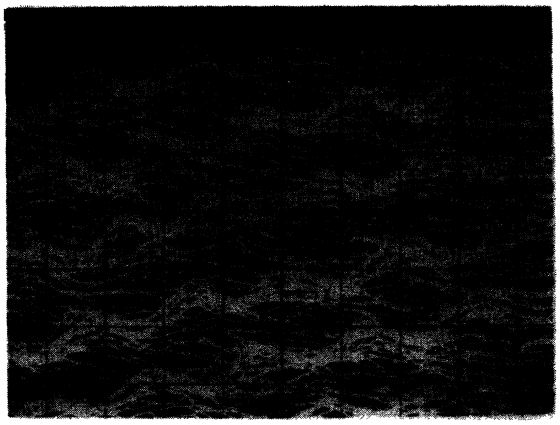

FIG. 6. STM image of CDW's in $1T$-TaS_2 at 77 K. The experimentally determined spacing of the hexagonal pattern is 11.51 ± 0.35 Å. The wavelength of the CDW is $\lambda_{CDW}=12.06$ Å$=\sqrt{13}a_0$, where $a_0=3.346$ Å. The CDW pattern has been photographed from the CRT of a storage oscilloscope. The horizontal motion across the surface corresponds to 6.6 Å per division of the graticule and the vertical motion to 6.6 Å per division. The z motion is superimposed on the y motion and corresponds to ≈ 3.5 Å per division. The result is a pseudo-three-dimensional image representing the CDW modulation of the image from the tunneling microscope operating in the constant current mode. The microscope settings were $I=5.5$ nA and bias voltage equal to 68 mV.

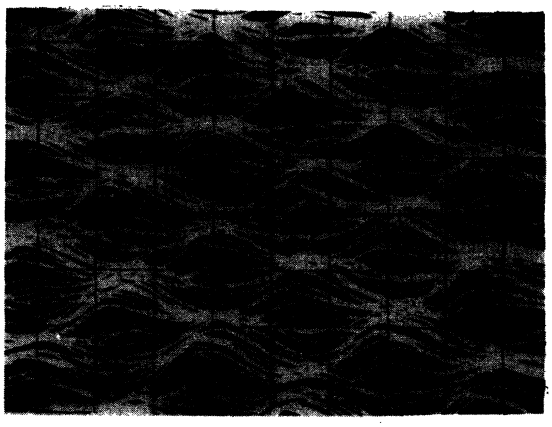

FIG. 7. STM image of CDW's in $1T$-$TaSe_2$ at 77 K. The experimentally determined spacing of the hexagonal pattern is 12.35 ± 0.25 Å. The wavelength of the CDW is $\lambda_{CDW}=12.43$ Å$=\sqrt{13}a_0$ where $a_0=3.447$ Å. The magnification is the same as used in obtaining the image shown in Fig. 6. The microscope settings were $I=3.7$ nA and bias voltage equal to 5.8 mV.

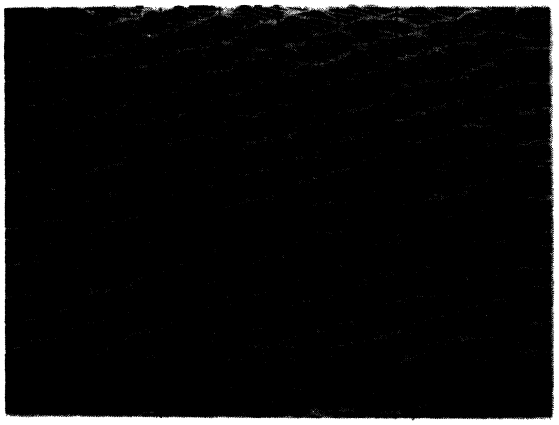

FIG. 8. STM image of atoms on the surface of $2H$-$TaSe_2$. The experimentally determined spacing of the atoms in the hexagonal pattern is 3.39 ± 0.13 Å. The spacing determined from electron diffraction measurements is $a_0=3.434$ Å. The magnification of the microscope is again the same as that used for Figs. 6 and 7. The microscope settings were $I=2.0$ nA and bias voltage equal to 40 mV. $T=77$ K.

of electron density associated with the atomic periodicity. In the case of $2H$-$TaSe_2$ careful adjustment of the microscope parameters have allowed us to obtain images exhibiting both the atomic periodicity and the CDW periodicity. The $2H$ phases have commensurate CDW's with $\lambda_{CDW}=3a_0$ so that the CDW structure will be coincident with every third row of atoms. Examples for $2H$-$TaSe_2$ at 77 K are shown in Figs. 9(a) and 9(b). In Fig. 9(a) one set of diagonal rows shows a spacing of 3.4 ± 0.2 Å close to the atomic spacing, $a_0=3.434$ Å, while the other set of rows at 120° shows a spacing of $3a_0$. Further adjustment of the gain and bias on the microscope produced a scan as shown in Fig. 9(b). In this case every third row of atoms shows an enhanced image while the intermediate two rows are weak. The two scans are from the same crystal, but at different locations on the surface. This demonstrates that the CDW images are generally weak in the $2H$ phases at least at 77 K. For most runs on $2H$-$TaSe_2$ the image is dominated by atoms as was shown in Fig. 8. Only rarely is the contrast sufficiently good to see the CDW. Computer enhancement of the data might help in this regard.

In the case of $2H$-TaS_2 the scans have so far only shown atoms as shown in Fig. 10. The spacing is 3.3 ± 0.2 Å again in agreement with the atomic spacing $a_0=3.315$ Å. For $2H$-TaS_2 the CDW reaches full amplitude below 77 K so that the absence of any CDW image may be associated with operating too close to T_C. We hope to explore this with a microscope operating at liquid-helium temperatures.

C. Images of CDW's in $4Hb$-TaS_2

The $4Hb$ phase of TaS_2 has four layers per unit cell with alternating layers of trigonal prismatic and octahe-

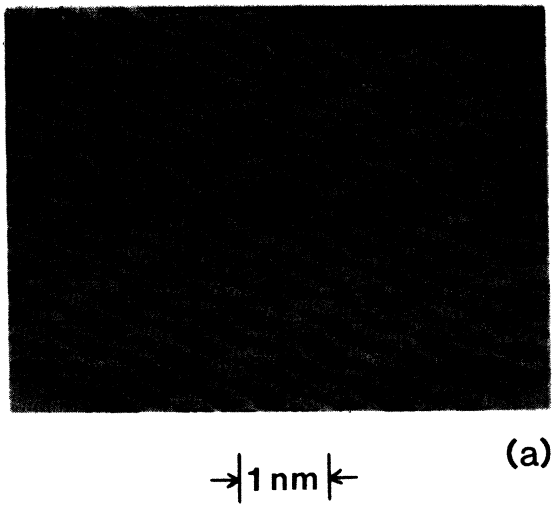

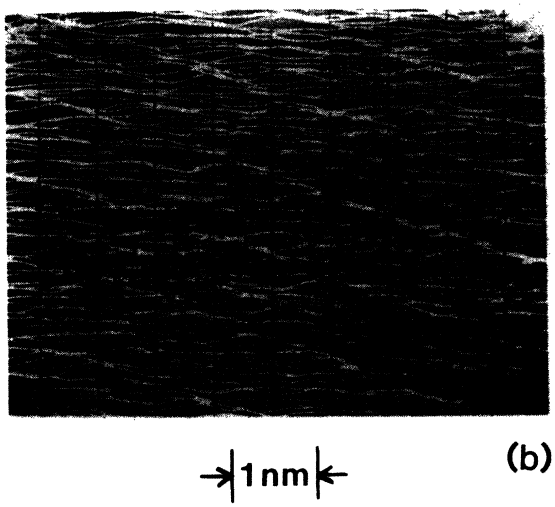

FIG. 9. STM images of atoms and CDW's on the surface of $2H$-$TaSe_2$. Careful adjustment of the STM has allowed the image to record modulations at both the atom and CDW wavelengths. (a) In one direction the image shows the atom spacing of 3.4±0.13 Å and in a direction oriented at 120° the CDW spacing of $3a_0$ dominates the pattern. The microscope settings were $I=2.0$ nA and bias voltage equal to 40 mV. (b) STM image obtained on the same crystal of $2H$-$TaSe_2$ used in (a) above, but on a different area. In this case every third row of atoms shows an enhanced image due to the added modulation of the CDW at a wavelength of $3a_0$. The microscope settings were $I=4.0$ nA and bias voltage equal to 31 mV.

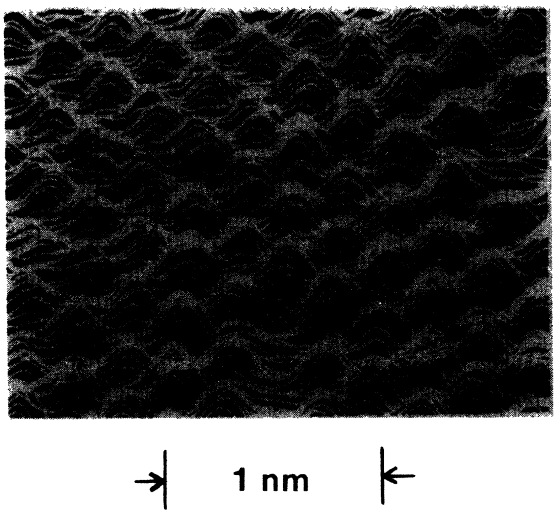

FIG. 10. STM image of atoms on the surface of $2H$-TaS_2 at 77 K. The x and y motions correspond to 3.3 Å per division on the graticule of the storage oscilloscope. A z motion of $\sim$ 1.8 Å per division is superimposed upon the y motion. The experimentally determined atom spacing is 3.27±0.07 Å compared to the value of $a_0=3.315$ Å determined by electron diffraction. The microscope settings were $I=3.0$ nA and bias voltage equal to 7 mV. Chalcogen vacancies appear at bottom of scan.

dral coordination. The two types of layers exhibit nearly independent CDW transitions with transition temperatures of 20 and 315 K, respectively. Therefore, at 77 K only the octahedral layers support a CDW associated with the 315 K transition. This is similar to the CDW in the $1T$ phase and has a wavelength $\lambda_{CDW}=\sqrt{13}a_0$. The resistance anomaly is weaker than in the $1T$ phase (see Fig. 11), but this is probably associated with the dominance of the conductivity in the trigonal prismatic layers. The resistance versus temperature is shown in Fig. 11 for current both parallel and perpendicular to the c axis.

Scans with the tunneling microscope on a cleaved $4Hb$-TaS_2 surface are shown in Fig. 12. Both patterns show a periodicity characteristic of the CDW with a wavelength $\lambda_{CDW}=\sqrt{13}a_0$. These crystals cleave extremely well and show optically smooth surfaces. However, we do not know whether the first surface layer is an octahedral or a trigonal prismatic layer. Regions which show poor definition of the CDW do not seem to show good atomic definition either. Some areas show islands of CDW formation as shown in Fig. 13 surrounded by an area where the surface is either rough or stepped on an atomic scale. This might involve an imperfect cleave where alternate layers are exposed at the surface, some type of domain structure, or just dirt or oxidation. Further accumulated data will be needed to analyze the possible interpretation of these boundaries.

Some areas of the $4Hb$-TaS_2 crystals show only atoms in the tunneling scans as shown in Fig. 14. These may correspond to areas where the trigonal prismatic layer is the top layer of the crystal, and consequently no CDW exists at the surface layer causing the atom pattern to be dominant.

IV. DISCUSSION

The tunneling microscope results reported in this paper are consistent with the conclusion that the CDW ampli-

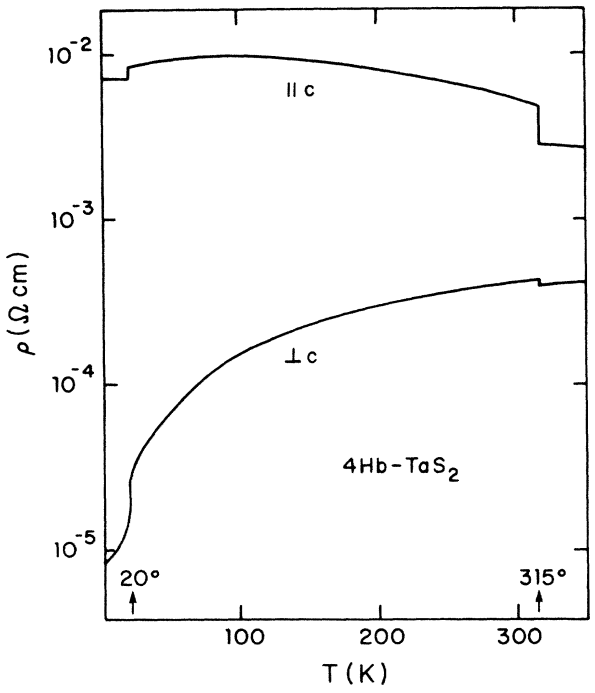

FIG. 11. Resistivity versus temperature measured parallel to the layers ($\perp$**c**) and perpendicular to the layers ($\|$**c**) for $4Hb$-TaS_2. The resistivity shows two discontinuities corresponding to independent CDW transitions at 315 K in the octahedrally coordinated layers and at 22 K in the trigonal prismatic layers. Data are from Ref. 42.

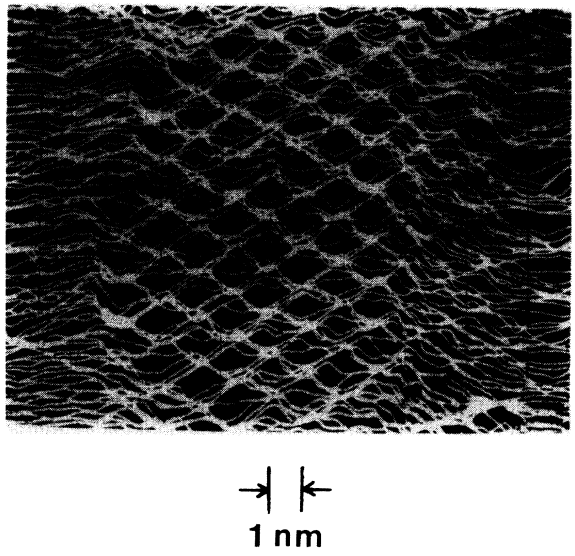

FIG. 13. STM image of a step on a cleaved surface of $4Hb$-TaS_2 at 77 K. A CDW pattern is observed on the middle layer which is the octahedrally coordinated layer. The regions on either side probably represent trigonal prismatic layers which support no CDW at 77 K. The magnification is $x=16.5$ Å per division, $y=16.5$ Å per division, with $z\approx 8.8$ Å per division superimposed on the y motion. The microscope settings were $I=3.6$ nA and bias voltage equal to 32 mV.

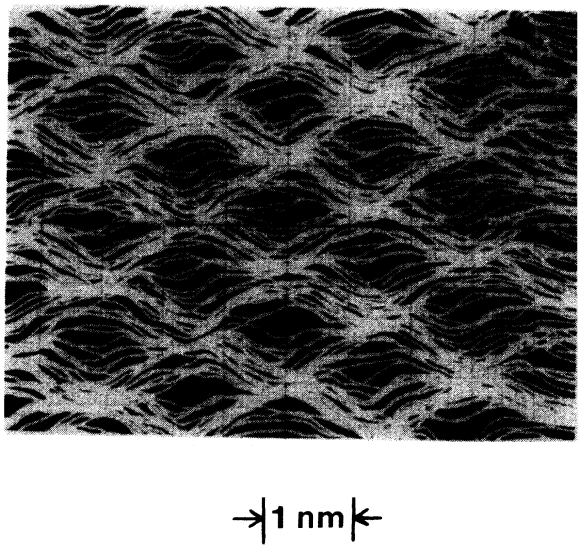

FIG. 12. STM image of CDW's in the octahedrally coordinated layer of $4Hb$-TaS_2 at 77 K. The experimentally determined spacing of the hexagonal pattern is 12.11 ± 0.12 Å. The magnification is $x=6.6$ Å per division, $y=6.6$ Å per division, with $z\approx 3.5$ Å per division superimposed on the y motion. The $\lambda_{CDW}=\sqrt{13}a_0$, where $a_0=3.33$ Å. The microscope settings were $I=3.1$ nA and bias voltage equal to 32 mV.

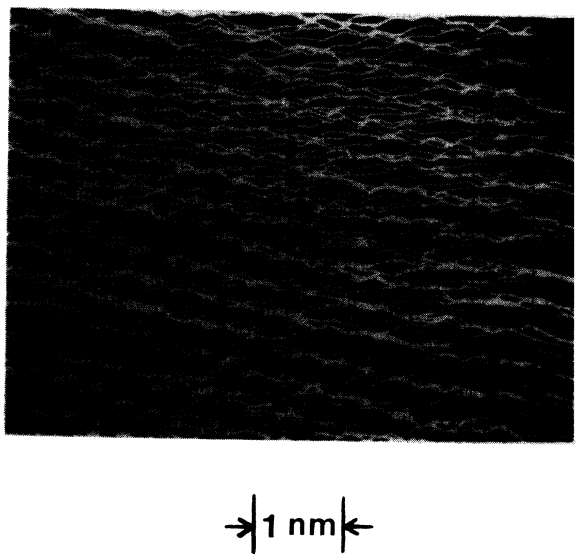

FIG. 14. STM image of the surface of $4Hb$-TaS_2 showing only atoms at an experimental spacing of 3.29 ± 0.16 Å. The magnification is $x=6.6$ Å per division, $y=6.6$ Å per division, with $z\approx 3.5$ Å per division superimposed on the y motion. This is the same magnification as used for the CDW image in Fig. 12. In this area of the crystal only the trigonal prismatic layer is probably exposed at the surface. The microscope settings were $I=4.0$ nA and bias voltage equal to 5.6 mV. $T=77$ K.

tude in the $1T$ phases is very strong while the CDW amplitude in the $2H$ phases is relatively weak. The formation of the CDW phase is accompanied by a lattice distortion which corresponds to displacements of the atoms in the range 0.1—0.2 Å. The resulting distorted unit cell and superlattice has been studied in great detail by electron,[2] x-ray,[24,25] and neutron diffraction[26–28] and the picture is now relatively complete for most of the phases of both TaS_2 and $TaSe_2$. Substantial progress has also been made in extending band-structure models to include the distorted phases and a reasonable analysis of the expected electronic structural changes can be made.

At present the resolution of the tunneling microscope is certainly not great enough to detect the variation in atom spacing caused by the CDW distortion. Detailed computer analysis of the data might accomplish this, but at present we have not carried out such an analysis. In this section we summarize the main results of the previous work on understanding the crystalline and electronic structure of the CDW phases and point out the general consistency of the tunneling results with the conclusions of previous work.

A. $1T$ phases

The crystal structure of the $1T$ phases has trigonal symmetry with one layer per unit cell possessing octahedral coordination of the Ta and Se atoms. The distorted structure[29,30] due to the CDW formation can be described by a six-pointed-star-shaped cluster of 13 Ta atoms as shown in Fig. 15. The displacements of the metal atoms from their substructure positions lie mainly within the metal planes while the sulfur or selenium atom displacements are mainly perpendicular to these planes. The sulfur or selenium atoms are essentially squeezed out of the clusters of 13 Ta atoms by the distortion. Both $1T$-TaS_2 and $1T$-$TaSe_2$ can be described by the star-shaped cluster, but the stacking along the c axis is different. $1T$-TaS_2 also shows a more complex two-stage transition to the commensurate CDW phases as a function of temperature while $1T$-$TaSe_2$ shows only one low-temperature incommensurate-to-commensurate phase transition at 473 K. The initial onset of the incommensurate CDW's in both $1T$-TaS_2 and $1T$-$TaSe_2$ is above 600 K.

From electron diffraction data Wilson *et al.*[2] concluded that $1T$-$TaSe_2$ had a commensurate superstructure with $a=b=a_0\sqrt{13}$ and $c'=12c_0$ or $13c_0$ where $a_0=3.478$ Å and $c_0=6.263$ Å. In the commensurate structure the CDW reciprocal lattice in the layer plane is rotated by 13.9° from the original unreconstructed unit cell. More recent work by Brouwer and Jellinek[29] finds that the true symmetry is triclinic, as determined from careful analysis of the twinning, and that the stacking along c is more complex than originally thought.

$1T$-TaS_2 exhibits a resistance anomaly and a first-order transition at 350 K where the triple CDW rotates by $\sim 11°$ and the CDW wave vector increases in length. This is an attempt to become commensurate and probably corresponds to an adjustment which allows $q_\perp$ to become commensurate while $q_{||}$ remains incommensurate. At 150 K q_{11} becomes commensurate and the rotation becomes equal to 13.9°. However, the c-axis stacking remains disordered in the low-temperature phase.

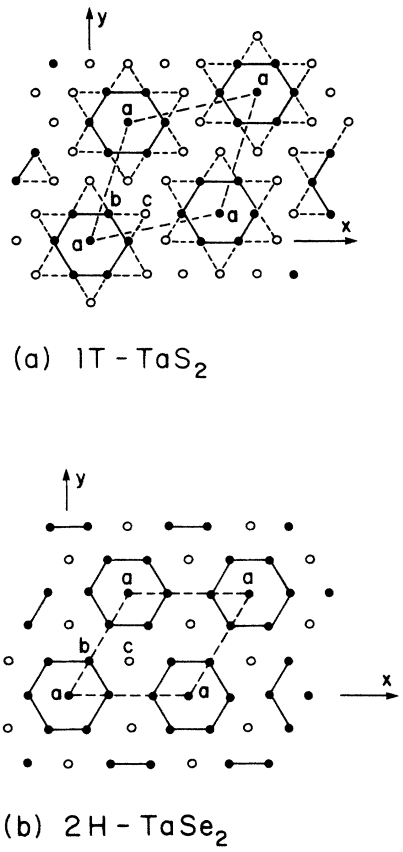

FIG. 15. Ta atom patterns representing the distorted lattice due to CDW formation in $1T$-$TaSe_2$ and $2H$-$TaSe_2$. (a) The pattern in $1T$-$TaSe_2$ is a six-pointed-star-shaped pattern made up of 13 Ta atoms. The electronic charge maximum occurs on the a-type atoms. The b-type and c-type atoms move toward the nearest a-type atom. See Ref. 33. (b) The Ta atom pattern of $2H$-$TaSe_2$ has three inequivalent atom sites of types a, b, and c with a contraction of the b-type atoms around the nearest a-type atom. See Ref. 33.

$1T$-TaS_2 also shows an additional modification of the nearly commensurate phase in the temperature range below 280 K. Tanda, Sambongi, and co-workers[31] have shown that this T phase occurs on both heating and cooling through the nearly-commensurate—to—commensurate transition, and undoubtedly the large hysteresis observed in the ρ versus T measurements on $1T$-TaS_2 is connected with the formation of the domain structure associated with this phase.

This more complicated structure in $1T$-TaS_2 would be an interesting study for the tunneling microscope when it can operate at intermediate temperatures. At 77 K both $1T$-TaS_2 and $1T$-$TaSe_2$ have essentially the same structure with a $\sqrt{13}\times\sqrt{13}$ unit cell rotated by 13.9° from the unreconstructed unit cell. The tunneling scans at 77 K on

$1T$-$TaSe_2$ and $1T$-TaS_2 both show the same $\sqrt{13}\times\sqrt{13}$ pattern, and so far no essential differences have been detected as seen by comparing Figs. 5 and 6. In both cases the crystals have been immersed in liquid nitrogen from room temperature by lowering the microscope into the liquid-nitrogen bath over a time scale of several minutes. Variations of the cooling rate or quenching of the crystals might show up differences in domain structure, but such studies have not been tried yet.

The effect of the CDW on the band structure of the $1T$ phases should be rather dramatic and should produce a large gapping of the Fermi surface with a reduction in carrier density. Band calculations of Myron and Freeman[32] showed that in the commensurate phase of $1T$-TaS_2 nesting occurred over substantial regions of the Fermi surface consistent with a large reduction in Fermi surface area. Smith *et al.*[33] have developed a band-structure model for $1T$-TaS_2 following work by Mattheiss[34] and by Doran and Woolley.[35] They simulate the effects of the CDW on the band structure and use the results to interpret their data from angle-resolved photoemission spectroscopy. Their analysis shows a major distortion of the band structure in which the *d* band derived from the Ta atoms collapses into three subband manifolds separated by gaps. The 13th electron resides in a very narrow band and can lead to a Mott-Anderson transition associated with the resistance rise observed in the helium temperature range (see Fig. 4). In the $\sqrt{13}\times\sqrt{13}$ unit cell of $1T$-TaS_2 there are three types of inequivalent atoms labeled a, b, and c in the proportion 1:6:6 as shown in the star-shaped clusters of Fig. 15. The atom-by-atom decomposition of the density of states (DOS) gives the total number of occupied electrons per atom on atoms of type a, b, and c as $n_a=1.455$, $n_b=1.311$, and $n_c=0.611$. The charge transfers involve a substantial fraction of an electron per atom consistent with a large-amplitude CDW. The results indicate that the CDW's appear to have a fairly uniform amplitude within the seven-atom cluster centered on atom a. One could reasonably conclude that the scanning tunneling pattern is the result of the influence on the tunneling current of the charge density surrounding atom a at the center of the seven-atom cluster.

B. $2H$ phases

The $2H$-$TaSe_2$ structure consists of the transition-metal atoms trigonally coordinated with the chalcogens in a hexagonal sandwich arrangement with two layers per unit cell. The CDW in the commensurate phase is characterized by a wave vector which is at one third of the smallest reciprocal-lattice vector, and from neutron diffraction[26] and electron diffraction[2] it was found that the CDW is a triple CDW forming a 120° star. This simply enlarges the unit cell nine times so that it will now contain $9\times6=54$ atoms.

Recent work[36] using convergent-beam electron diffraction has shown that the commensurate CDW state has orthorhombic symmetry in contrast to the hexagonal symmetry determined from neutron diffraction.[26] This resulted from the presence of a microstructure of orthorhombic domains oriented in three equivalent directions relative to the underlying hexagonal sublattice. These are averaged by the large neutron probe while the electron-diffraction experiment was able to look at a single domain. The scanning tunneling microscope looks at a single domain, but resolution and accuracy are not at a point where the subtle variations in the CDW superlattice can be detected.

The triple CDW forms first in an incommensurate state characterized by a second-order (or nearly second-order) transition at 122.3 K followed by a first-order transition near 90 K below which the CDW superlattice is commensurate. The 3×3 unit cell of $2H$-$TaSe_2$ in the commensurate CDW phase has three types of inequivalent Ta atoms designated a, b, and c in Fig. 15 and having numerical proportions 1:6:2. The atomic displacements and charge transfer again involve a seven-atom cluster with one atom of type a and six surrounding atoms of type b.

Doran and Woolley[35] have carried out a band-structure calculation for the 3×3 CDW state in the $2H$ phase and have examined the effects of the CDW amplitude on the DOS and the electronic energy. The formation of the CDW results in substantial band folding and Fermi-surface rearrangement, but it does not result in a large change of conductivity. The band calculation shows the existence of six doubly degenerate cylinders containing electrons rather than holes as calculated for the high-temperature band structure and consistent with the change in sign of the Hall coefficient on passing below the CDW transition temperature. The overall shape of the DOS is similar in both the normal and the CDW phase and the Fermi level lies just above the main peak in the DOS. This main peak probably plays an important role in stabilization of the CDW amplitude and becomes broader and smaller as the CDW amplitude is increased. The CDW does not open just one gap at the Fermi energy, but band degeneracies are lifted and bands are shifted in a number of places. The overall Fermi-surface rearrangement is consistent with de Haas–van Alphen[37] and Shubnikov–de Haas[22] experiments which show up to 11 frequencies exhibiting an angular dependence characteristic of undulating cylinders. Wilson[38] has in fact used a band-folding model to fit most of these frequencies.

This modification and rearrangement of the band structure does not involve the dramatic changes in band structure observed for the $1T$ phase. This is also confirmed in the model band-structure calculation used by Smith *et al.*[33] to analyze their photoemission data. The DOS as decomposed for the inequivalent a, b, and c atoms show no gaps opening in the subband manifolds with the main modification corresponding to a change in the DOS at the bottom of the band. The numbers of Ta *d* electrons on each of the inequivalent sites are $n_a=1.014$, $n_b=1.005$, and $n_c=0.977$, where the departures from unity are relatively small.

All of these calculations and models confirm that the CDW and associated charge transfer are relatively weak in the $2H$ phase of $TaSe_2$. However, the scanning tunneling results show that it is strong enough to modify the tunneling current sufficiently to produce an image with a $3a_0$ periodicity, but that this does not dominate over the atomic periodicity as was the case in the $1T$ phases. The

amplitude of this $3a_0$ modulation also corresponds to ≤ 0.3 Å and is on the same order as the atomic modulation in contrast to the giant modulation observed for the $1T$ CDW in the tunneling microscope.

We do not as yet understand the variations in the CDW images and the fact that sometimes only the atom periodicity can be detected as shown in Fig. 8. In the temperature range just above the lock-in temperature of 90 K fairly complex discommensurations and domains can be observed and these also relate to the exact details of the CDW ground state in $2H$-$TaSe_2$. Different crystals and cooling rates may produce microscopic differences in the resulting scanning images but we have not as yet developed enough statistics on such variations. Wilson and Vincent[39] and Wilson[40] have done extensive work on analyzing the CDW phasing and discommensuration arrays in $2H$-$TaSe_2$ and in view of recent electron diffraction intensity data by Bird *et al.*[41] a new phasing solution having a charge hill center between two Ta atoms will have to be considered

The ability of the scanning tunneling microscope to see both the atom periodicity and the superimposed CDW charge density should offer a good potential for examining details of the overall charge-density distribution in the CDW ground state of $2H$-$TaSe_2$. A temperature variable microscope in the range 90—120 K would also be highly useful in studying the formation of discommensurations in $2H$-$TaSe_2$.

$2H$-TaS_2 has a peak in susceptibility at 80 K, a break in resistivity at 75 K, and a change in sign of the Hall resistivity between 65 and 55 K. Careful resistivity measurements by Tidman *et al.*[42] show an abrupt change in ρ_{11} at 75.3 K leading to the conclusion that the Fermi-surface modification occurs at or below this temperature.

Superlattice spots are observed by electron diffraction at 66 K and remain unchanged down to at least 16 K. The superlattice reflections give a period of $\mathbf{a}_0^*/3$ where $\mathbf{a}_0^*$ is the reciprocal lattice vector above the transition. At low temperature the ground state should be a $3a_0 \times 3a_0$ superlattice very similar to that of $2H$-$TaSe_2$. The scanning tunneling microscope images taken at 77 K show only atoms at a spacing of 3.3 ± 0.2 Å, well within range of the value 3.310 Å measured for the undistorted lattice. The absence of any CDW amplitude is probably consistent with the fact that the CDW has not developed sufficient amplitude at 77 K to modify the electron density.

$2H$-TaS_2 is clearly a crystal which should be studied in a helium temperature scanning tunneling microscope where the amplitude of the CDW should be fully developed. Shubnikov—de Haas and de Haas—van Alphen experiments[23] at 1.1 K show many low frequencies consistent with the rearrangement of the Fermi surface expected for the CDW phase.

C. $4Hb$-TaS_2

This polytype has four layers per unit cell consisting of alternating layers of trigonal prismatic coordination and octahedral coordination TaS_2. Its properties are, to a large extent, a composite of those of the pure octahedral ($1T$) and pure trigonal prismatic ($2H$) materials.[2,43] The crystals exhibit two CDW transitions at temperatures of 315 and 22 K, respectively. At the high-temperature transition two $\sqrt{13}a_0$ rotated superlattices appear and this is generally associated with CDW formation in the octahedral layers. At the low temperature transition an incommensurate 3×3 superlattice is observed to form associated with the trigonal prismatic layers.

Electron diffraction results give a ratio $q'/a^* = 0.263$ for the octahedral superlattice cell where q' is the superlattice wave vector and a^* is the in-the-layer reciprocal-lattice vector. The $1T$ polytype has a q'/a^* equal to 0.288 while the precise commensurate value should be 0.277. This fact along with preliminary band-structure calculations[44] suggests a small transfer of electrons out of the octahedral layers into the trigonal prismatic layers. This requires a small adjustment of the Fermi surface, but from the standpoint of the tunneling scans at 77 K the pattern should be approximately the same as observed in the $1T$ phase if the octahedral layers are being observed. This is indeed the case as shown in Fig. 12, and the effective amplitude as measured by the tip deflection is again extremely strong at ~ 2 Å. From the electron-diffraction intensities it is thought that the octahedral CDW distortion is weaker in the $4Hb$ phase than in the $1T$ phase. However, the tunneling scan shows that the modified charge density associated with the CDW is sufficiently strong that it completely dominates the periodicity in the tunneling scan: no atom periodicities are observed in the CDW regions of the crystal.

At 77 K the trigonal prismatic layers should contain no CDW component, and this may account for areas of the crystal which show only atom periodicities as shown in Fig. 14. So far we have not resolved well-defined boundaries that separate each type of area other than the rather poorly defined boundaries that were shown in Fig. 13. The $4Hb$ phase is clearly a candidate for study at helium temperatures where CDW's are present in both the octahedral and trigonal prismatic layers.

D. Atom diffraction data on $1T$-TaS_2

Cantini *et al.*[45] have carried out diffraction experiments on $1T$-TaS_2 using a supersonic beam of helium atoms. At ~ 80 K they observed satellite peaks associated with the $\sqrt{13} \times \sqrt{13}$ superlattice which had approximately the same intensity as the main peaks. This seems to indicate a fairly large periodic deformation of the surface at the CDW wavelength resulting from both displacement of the sulfur ions and a change in their atomic radii. This in turn is related to the charge transfer occurring between the Ta atoms, and all of these effects cannot be easily separated. The vertical displacement of the sulfur atoms was estimated from model fits of the diffraction data and gave values ranging from -0.11 to $+0.15$ Å.

This will definitely contribute to the scanning tunneling tip defection and must be taken into account. The charge modulation on the Ta atoms will also propagate to the surface, and the tunneling tip will respond to a combination of the two effects. More detailed models will be needed, but the diffraction results clearly point to the same conclusion as the STM results; both indicate a

strong perturbation at the surface caused by the CDW. However, the tunneling tip deflection at ~ 2 Å is much larger than the displacement indicated in the He atom diffraction experiment.

V. CONCLUSIONS

We have shown that images of the charge-density-wave structure in layered-structure dichalcogenides can be obtained with the scanning tunneling microscope. In the $1T$ phases of $TaSe_2$ and TaS_2 the CDW modulation at a wavelength $\lambda_{CDW}=\sqrt{13}a_0$ produces a surprisingly large deflection of the tunneling tip which completely dominates over the charge-density modulation at the atomic wavelength. In $4Hb$-TaS_2 at 77 K only the octahedrally coordinated layers exhibit a CDW and this also dominates the tunneling scan in some areas of the crystal while other areas show only atoms.

From previous theoretical and experimental work on the $1T$ phases the charge transfer associated with the CDW formation is expected to be large corresponding to a major fraction of an electron. In this respect the tunneling response is consistent, but a deflection in the z motion of ~ 2 Å is abnormally large. Modifications in the local tunneling density of states or unusual structure in the surface electronic wave function may be involved, but more experimental work along with theoretical analysis must be carried out. Preliminary results show that the amplitude is a function of applied bias voltage in the range 8—70 mV, and this variation will be analyzed in more detail, but the amplitude remains large over the entire voltage range.

In contrast, the $2H$ phases of $TaSe_2$ and TaS_2 show a scanning tunneling image in which the dominant modulation occurs at the atomic wavelength. At 77 K $TaSe_2$ has a well-formed commensurate CDW at a wavelength $\lambda_{CDW}=3a_0$. For precise adjustment of the STM on high-quality surface areas of the crystal the CDW modulation can be resolved in addition to the atomic modulation. These results are again consistent with previous theoretical and experimental work which concludes that in the $2H$ phases the charge transfer associated with CDW formation should be quite small. In $2H$-TaS_2 at 77 K the CDW is just near onset and the Fermi surface modification is not complete until $T \lesssim 75$ K. The tunneling scans at 77 K show only atoms in this case. The amplitude of the z deflection is ~ 0.3 Å.

Overall we conclude that the cleaved layer structure surfaces are excellent for direct imaging of both atoms and CDW's with the STM. The large amplitude may be associated with special features of the CDW charge density and this will have to be investigated in comparison to some other non-CDW materials. The Ta-based layer structures do not oxidize rapidly and this fact combined with the large amplitude response makes them excellent crystals for testing the operation of the STM. The data reported here are analog pictures taken from a storage oscilloscope. The quality of the images indicate that digital data collection and image processing will provide significantly more information on CDW structure.

ACKNOWLEDGMENTS

We thank V. Celli, J. Tersoff, J. A. Golovchenko, and N. V. Smith for useful comments and discussion on these results. The U.S. Department of Energy Grant No. DE-FG05-84ER45072 supported three of us (C.G.S., W.W.McN., and R.V.C.,) and provided supplies and equipment. The National Science Foundation Grant No. DMR83-03623 supported one of us (P.K.H.) and provided funds for construction of the electronic equipment. The U.S. Office of Naval Research supported one of us (B.D.) and provided funds for construction of the microscope stage.

[1]Gerd Binning and Heinrich Rohrer, Sci. Am. **253**, 50 (1985).
[2]J. A. Wilson, F. J. Di Salvo, and S. Mahajan, Adv. Phys. **24**, 117 (1975).
[3]R. V. Coleman, B. Drake, P. K. Hansma, and G. Slough, Phys. Rev. Lett. **55**, 394 (1985).
[4]R. Young, Phys. Today **24**, 42 (1971).
[5]R. Young, J. Ward, and F. Scire, Rev. Sci. Instrum. **47**, 1303 (1976).
[6]G. Binnig, H. Rohrer, Ch. Gerber, and E. Weibel, Phys. Rev. Lett. **49**, 57 (1982).
[7]G. Binnig and H. Rohrer, Surf. Sci. **126**, 236 (1983).
[8]G. K. Binnig, H. Rohrer, Ch. Gerber, and E. Stoll, Surf. Sci. **144**, 321 (1984).
[9]G. Binnig, H. Rohrer, Ch. Gerber, and E. Weibel, Phys. Rev. Lett. **50**, 120 (1983).
[10]J. A. Golovchenko, Bull. Am. Phys. Soc. **30**, 251 (1985).
[11]S. A. Elrod, A. L. de Lozanne, and C. R. Quate, Appl. Phys. Lett. **45**, 1240 (1984).
[12]C. Quate, Bull. Am. Phys. Soc. **45**, 251 (1985).
[13]G. Binnig, Bull. Am. Phys. Soc. **30**, 251 (1985).
[14]B. Drake, R. Sonnenfeld, J. Schneir, P. K. Hansma, G. Slough, and R. V. Coleman, Rev. Sci. Instrum. **57**, 441 (1986).
[15]J. Moreland, S. Alexander, M. Cox, R. Sonnenfeld, and P. K. Hansma, Appl. Phys. Lett. **43**, 387 (1983).
[16]J. Moreland and P. K. Hansma, Rev. Sci. Instrum. **55**, 399 (1984).
[17]J. Moreland, J. Drucker, P. K. Hansma, J. P. Kotthaus, A. Adams, and R. Kvaas, Appl. Phys. Lett. **45**, 104 (1984).
[18]R. Sonnenfeld, J. Moreland, P. K. Hansma, A. Adams, and R. Kvaas, J. Appl. Phys. **58**, 392 (1985).
[19]Channel Industries, Santa Barbara, CA.
[20]Piezoelectric Technology Data for Designers, available from Vernitron, Bedford, Ohio.
[21]Channel 5400 is similar to PZT4; Channel 5800 is similar to PZT8 according to M. Cullen of Channel Industries.
[22]R. M. Fleming and R. V. Coleman, Phys. Rev. B **16**, 302 (1977).
[23]S. J. Hillenius and R. V. Coleman, Phys. Rev. B **18**, 3790 (1978).

[24]P. M. Williams, G. S. Parry, and C. B. Scruby, Philos. Mag. **29**, 695 (1974).
[25]R. Moret and E. Tronc, Physica **99B**, 56 (1980).
[26]D. E. Moncton, J. D. Axe, and F. J. Di Salvo, Phys. Rev. Lett. **35**, 120 (1975); Phys. Rev. B **16**, 801 (1977).
[27]F. J. Di Salvo, D. E. Moncton, J. A. Wilson, and S. Mahajan, Phys. Rev. B **14**, 1543 (1976).
[28]D. E. Moncton, F. J. Di Salvo, J. D. Axe, L. J. Sham, and B. R. Patton, Phys. Rev. B **14**, 3432 (1976).
[29]R. Brouwer and F. Jellinek, Physica **99B**, 51 (1980).
[30]K. K. Fung, J. W. Steeds, and J. A. Eades, Physica **99B**, 47 (1980).
[31]Satoshi Tanda, Takashi Sambongi, Toshiro Tani, and Shoji Tanaka, J. Phys. Soc. Jpn. **53**, 476 (1984).
[32]H. W. Myron and A. J. Freeman, Phys. Rev. B **11**, 2735 (1975).
[33]N. V. Smith, S. D. Kevan, and F. J. Di Salvo, J. Phys. C **18**, 3175 (1985).
[34]L. F. Mattheiss, Phys. Rev. B **8**, 3719 (1973).
[35]N. J. Doran and A. M. Woolley, J. Phys. C **14**, 4257 (1981).
[36]K. K. Fung, S. McKernan, J. W. Steeds, and J. A. Wilson, J. Phys. C **14**, 5417 (1981).
[37]J. E. Greabner, Solid State Commun. **21**, 353 (1977).
[38]J. A. Wilson, Phys. Rev. B **15**, 5746 (1977).
[39]J. A. Wilson and R. Vincent, J. Phys. F **14**, 123 (1984).
[40]J. A. Wilson, J. Phys. F **15**, 591 (1985).
[41]D. M. Bird, S. McKernan, and J. W. Steeds, J. Phys. C **18**, 499 (1985).
[42]J. P. Tidman, O. Singh, A. E. Curzon, and R. F. Frindt, Philos. Mag. **30**, 1191 (1974).
[43]R. H. Friend, D. Jérome, F. F. Frindt, A. J. Grant, and A. D. Yoffe, J. Phys. C **10**, 1013 (1977).
[44]Wexter and Woolley (unpublished).
[45]P. Cantini, G. Boato, and R. Colella, Physica **99B**, 59 (1980).

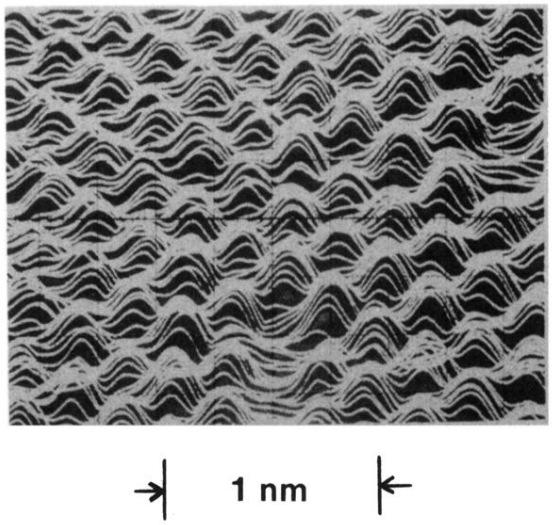

FIG. 10. STM image of atoms on the surface of $2H$-TaS_2 at 77 K. The x and y motions correspond to 3.3 Å per division on the graticule of the storage oscilloscope. A z motion of $\sim$ 1.8 Å per division is superimposed upon the y motion. The experimentally determined atom spacing is 3.27 ± 0.07 Å compared to the value of $a_0=3.315$ Å determined by electron diffraction. The microscope settings were $I=3.0$ nA and bias voltage equal to 7 mV. Chalcogen vacancies appear at bottom of scan.

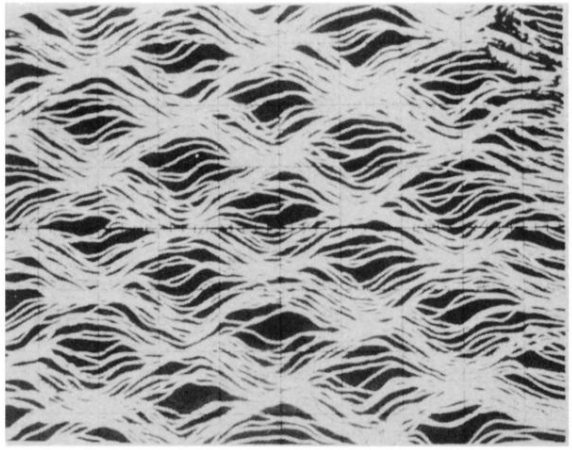

FIG. 12. STM image of CDW's in the octahedrally coordinated layer of $4Hb$-TaS_2 at 77 K. The experimentally determined spacing of the hexagonal pattern is 12.11 ± 0.12 Å. The magnification is $x = 6.6$ Å per division, $y = 6.6$ Å per division, with $z \approx 3.5$ Å per division superimposed on the y motion. The $\lambda_{\mathrm{CDW}} = \sqrt{13} a_0$, where $a_0 = 3.33$ Å. The microscope settings were $I = 3.1$ nA and bias voltage equal to 32 mV.

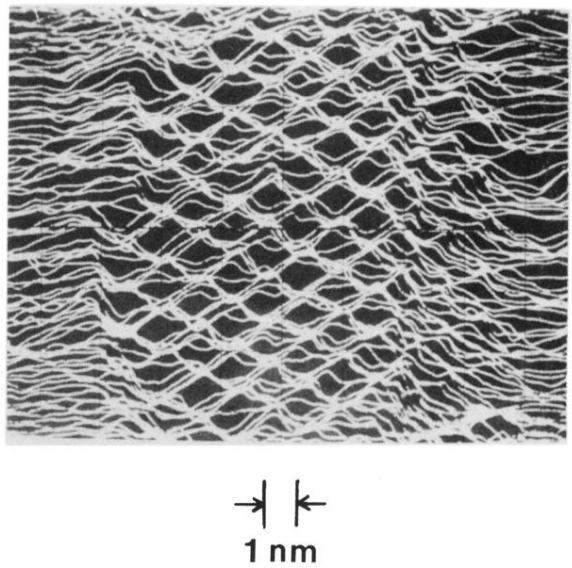

FIG. 13. STM image of a step on a cleaved surface of $4Hb$-TaS_2 at 77 K. A CDW pattern is observed on the middle layer which is the octahedrally coordinated layer. The regions on either side probably represent trigonal prismatic layers which support no CDW at 77 K. The magnification is $x = 16.5$ Å per division, $y = 16.5$ Å per division, with $z \approx 8.8$ Å per division superimposed on the y motion. The microscope settings were $I = 3.6$ nA and bias voltage equal to 32 mV.

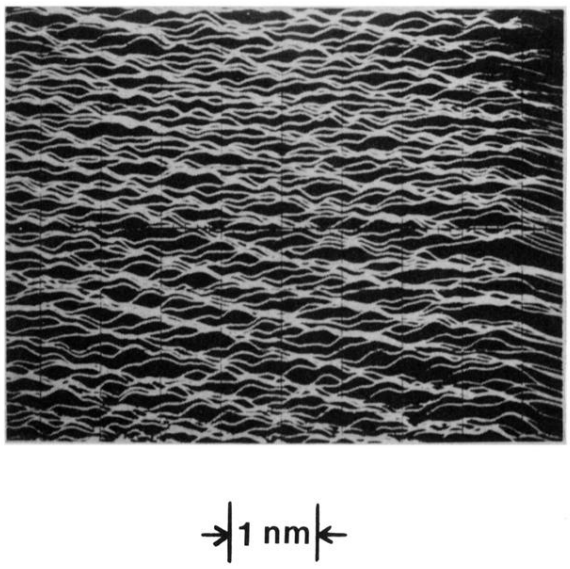

FIG. 14. STM image of the surface of $4Hb$-TaS_2 showing only atoms at an experimental spacing of 3.29 ± 0.16 Å. The magnification is $x = 6.6$ Å per division, $y = 6.6$ Å per division, with $z \approx 3.5$ Å per division superimposed on the y motion. This is the same magnification as used for the CDW image in Fig. 12. In this area of the crystal only the trigonal prismatic layer is probably exposed at the surface. The microscope settings were $I = 4.0$ nA and bias voltage equal to 5.6 mV. $T = 77$ K.

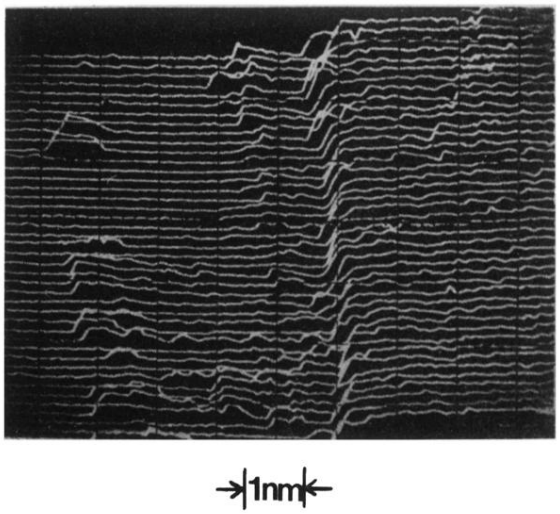

FIG. 3. STM image of a cleavage step on a $2H$-$TaSe_2$ crystal surface at 77 K. The step height is 17.0±2.1 Å corresponding to 3 atomic layers. The microscope was set for $I=2$ nA and bias voltage equal to 40 mV.

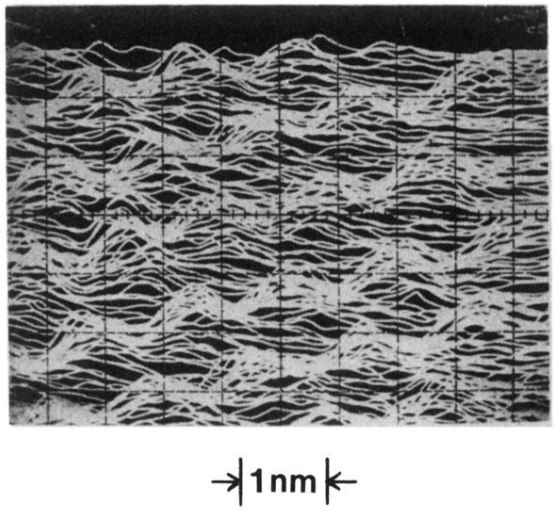

FIG. 6. STM image of CDW's in $1T$-TaS_2 at 77 K. The experimentally determined spacing of the hexagonal pattern is 11.51 ± 0.35 Å. The wavelength of the CDW is $\lambda_{CDW} = 12.06$ Å $= \sqrt{13} a_0$, where $a_0 = 3.346$ Å. The CDW pattern has been photographed from the CRT of a storage oscilloscope. The horizontal motion across the surface corresponds to 6.6 Å per division of the graticule and the vertical motion to 6.6 Å per division. The z motion is superimposed on the y motion and corresponds to ≈ 3.5 Å per division. The result is a pseudo-three-dimensional image representing the CDW modulation of the image from the tunneling microscope operating in the constant current mode. The microscope settings were $I = 5.5$ nA and bias voltage equal to 68 mV.

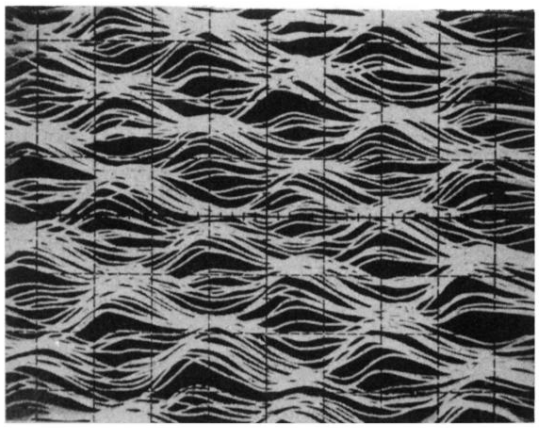

FIG. 7. STM image of CDW's in 1T-$TaSe_2$ at 77 K. The experimentally determined spacing of the hexagonal pattern is 12.35 ± 0.25 Å. The wavelength of the CDW is $\lambda_{CDW} = 12.43$ Å $= \sqrt{13} a_0$ where $a_0 = 3.447$ Å. The magnification is the same as used in obtaining the image shown in Fig. 6. The microscope settings were $I = 3.7$ nA and bias voltage equal to 5.8 mV.

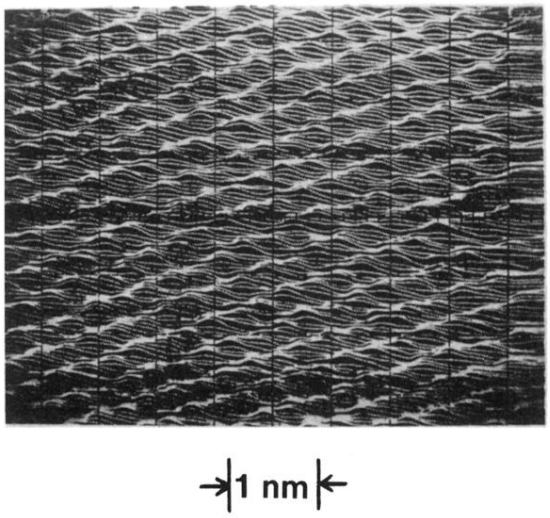

FIG. 8. STM image of atoms on the surface of $2H$-$TaSe_2$. The experimentally determined spacing of the atoms in the hexagonal pattern is 3.39 ± 0.13 Å. The spacing determined from electron diffraction measurements is $a_0 = 3.434$ Å. The magnification of the microscope is again the same as that used for Figs. 6 and 7. The microscope settings were $I = 2.0$ nA and bias voltage equal to 40 mV. $T = 77$ K.

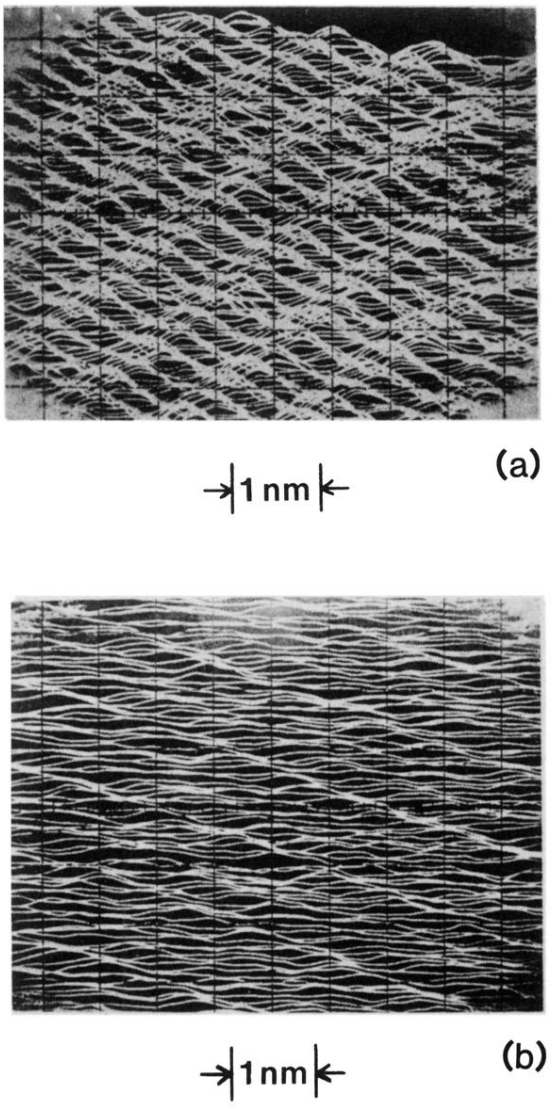

FIG. 9. STM images of atoms and CDW's on the surface of $2H$-$TaSe_2$. Careful adjustment of the STM has allowed the image to record modulations at both the atom and CDW wavelengths. (a) In one direction the image shows the atom spacing of 3.4 ± 0.13 Å and in a direction oriented at 120° the CDW spacing of $3a_0$ dominates the pattern. The microscope settings were $I=2.0$ nA and bias voltage equal to 40 mV. (b) STM image obtained on the same crystal of $2H$-$TaSe_2$ used in (a) above, but on a different area. In this case every third row of atoms shows an enhanced image due to the added modulation of the CDW at a wavelength of $3a_0$. The microscope settings were $I=4.0$ nA and bias voltage equal to 31 mV.